Appl. Phys. B 43, 189–195 (1987)

Applied Physics B Photophysics and Laser Chemistry

Calculation of Geometrical Changes in Cylindrical Copper Hollow Cathodes due to Sputtering

J. Hamisch and J. de la Rosa

Technische Universität, Optisches Institut, D-1000 Berlin 12, Fed. Rep. Germany

Received 3 October 1986/Accepted 15 January 1987

Abstract. To find the reasons for the distortion of a cylindrical hollow cathode into a row of hollow spheres, the system of diffusion equations for the three most important types of particles in the hollow cathode discharge is solved, taking into consideration the essential source terms. In qualitative agreement with the experiments, the results show inhomogeneities of the cathode erosion at the cathode edges and at the boundary between hollow cathode discharge and normal glow discharge areas.

PACS: 52.80.Hc, 79.20.Nc, 42.55.Hq

Cylindrical hollow cathodes are used to evaporate materials for spectroscopic analysis [1], for spectral lamps and for metal vapor lasers. For example, a copper ion laser consists of several copper hollow cathode segments alternating with anode segments [2].

The necessary copper atoms are produced by sputtering of the hollow cathodes. The atoms are ionized and excited to the upper laser level by charge transfer collisions with the ions of the discharge gas (helium or neon). It is known from experiments, that in hollow cathodes the spatial distributions of cathode erosion by sputtering and of copper condensation on the cathode must be different. This imbalance is indicated by a change of the cathode geometry, which moreover results in changing discharge characteristics and decreasing laser power. For example, cylindrical cathodes assume a shape similar to hollow spheres [1, 3–5]. This distortion appears in cylinders closed on one side [1, 3, 4] as well as in cylinders, which are open on both sides. In long cylinders [4, 5] several hollow spheres appear in a row, their number depending on the ratio of length and diameter of the cylinder. In short cylinders only one hollow sphere develops. In this case the geometry tends to stabilize [3, 5]. A stable cathode geometry would be good for a stable operation of the copper ion laser.

To find some reasons for the distortion of the cathodes, it was tried with certain assumptions to calculate the geometrical change, respectively, to calculate the mentioned different distributions of the cathode erosion by sputtering and of the copper condensation. This imbalance can occur only, if the spatial distributions of sputtering and condensing particles are different. This means that the spatial distributions of copper atoms, copper ions and gas ions had to be calculated. Especially the axial dependences of the particle densities are important to know.

Up to now calculations were made only for mean particle densities in hollow-cathode discharges [6, 7] and for radial dependences of the particle densities in slotted [6] and in cylindrical hollow cathodes [8]. To calculate the mean particle densities, the model of rate equations was applied. To calculate the radial dependences, diffusion terms were added to the rate equations, i.e., diffusion equations including several terms for sources and losses had been solved either analytically with some approximations [6] or numerically by a forward integration method [8].

To allow for a comparison of the calculations, which are described in the following chapters, to experimental results for the cathode erosion, the experimental parameters were chosen as given in [5] for a single cathode, which is open on both sides, i.e., which is usable in a laser arrangement:

cathode length $L = 4$ cm,

cathode diameter $2R = 0.4$ cm,

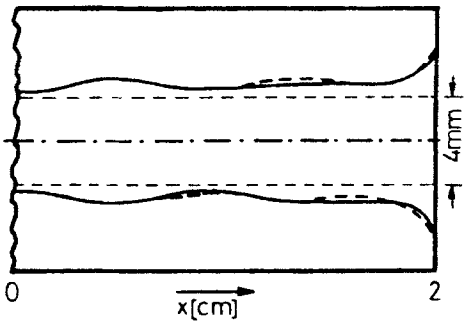

Fig. 1. Longitudinal section of a cylindrical hollow cathode after 200 h in a dc current discharge [9]. Both nearly symmetric halfs of the cathode are projected on top of each other. x is the axial direction ($x=0$ in the centre of the cathode)

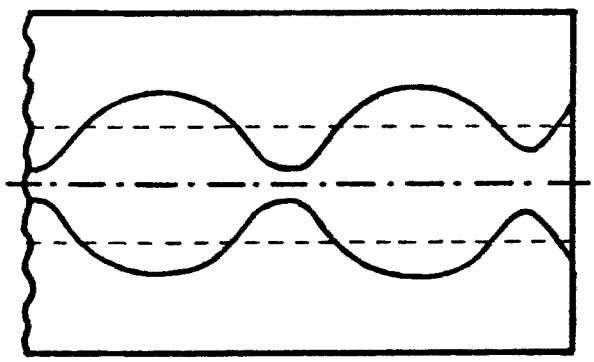

Fig. 2. Longitudinal section of the cathode, shown in Fig. 1, after about 200 additional hours in the discharge

neon pressure $p_{Ne}=8$ mbar,
discharge current $I=0.3$ A,
discharge voltage $U=300$ V.

Anodes had been next to the cathode on both sides. After an operation period of 200 h with dc current a change in geometry could be seen, as shown in Fig. 1 [9], which after a longer operation period developed into the formation of 4 hollow spheres [5] (Fig. 2).

Theory

The negative glow region inside the hollow cathode is nearly field-free, because the voltage drop across the small cathode fall at the cathode walls nearly equals the discharge voltage. The remaining small electrical field in the negative glow is neglected. Thus the spatial distributions of copper atoms, copper ions and gas ions are determined by the diffusion equation for the corresponding particle density N

$$\partial N/\partial t = V\cdot(DVN)+S = VD\cdot VN + D\cdot \Delta N + S\,. \qquad (1)$$

D is the diffusion coefficient for the corresponding particle type, which depends on the position, too. S is a source term, which includes various mechanisms of particle generation and losses. Now a steady state and an acimutal independence of N and D is assumed

$$\frac{\partial D}{\partial r}\cdot\frac{\partial N}{\partial r} + D\left(\frac{1}{r}\cdot\frac{\partial N}{\partial r}+\frac{\partial^2 N}{\partial r^2}\right) + \frac{\partial D}{\partial x}\cdot\frac{\partial N}{\partial x} + D\cdot\frac{\partial^2 N}{\partial x^2} + S = 0\,, \qquad (2)$$

where x is the axial coordinate in the cylindrical cathode. Now the radial distribution of the particle density is approximated by a mean particle density depending on the position x. The diffusion coefficient is treated in the same way. Then, D is the average diffusion coefficient in a cross section. The radial diffusion of the particles to the walls is not neglected. It is expressed by an additional loss term $-N/\tau$, where $\tau=1/(HD)$ is the average diffusive life time. The factor H is determined by the boundary conditions (loss of particles at the cathode walls), i.e., by the geometry of the cathode. For a cylinder with radius R (which is approximately the radius of the negative glow) it is $H=(2.405/R)^2$, neglecting boundaries in the axial direction [10]. Now we obtain from (2)

$$-\frac{N}{\tau}+\frac{\partial D}{\partial x}\cdot\frac{\partial N}{\partial x}+D\frac{\partial^2 N}{\partial x^2}+S=0\,. \qquad (3)$$

Thus (1) is reduced to an ordinary differential equation, which determines the average particle density N as a function of the position x. Considering (3) without the differential terms, this corresponds to the rate equations, which include only mean particle densities [7]. In this respect (3) can be interpreted as an extension of the rate equations by diffusion losses in the axial direction.

Equation (3) must be given for the three important particle types, which are indicated as follows

$$Cu\rightarrow 1,\ Cu^+\rightarrow 2,\ Ne^+\rightarrow 3\,.$$

Further we define $\partial N/\partial x = N'$ and $\partial D/\partial x = D'$. Equation (3) is modified for the Cu atoms, to take into account that a fraction of the Cu atoms is reflected after the diffusion to the walls. The chance that they will stick to the surface is the sticking coefficient A_1 [8]. Copper ions are not reflected as ions but at the most as atoms (due to recombination) i.e.,

$$N_1'' + D_1'N_1'/D_1 - HA_1N_1 + S_1/D_1 = 0\,, \qquad (4)$$

$$N_2'' + D_2'N_2'/D_2 - HN_2 + S_2/D_2 = 0\,, \qquad (5)$$

$$N_3'' + D_3'N_3'/D_3 - HN_3 + S_3/D_3 = 0\,. \qquad (6)$$

Because the source terms S_1, S_2 and S_3 are functions of N_1, N_2 and N_3, these differential equ-

ations are coupled. As has been done in [7], the following mechanisms of particle generation and losses are considered. Copper atoms are generated by sputtering at the cathode walls, and they are annihilated by charge transfer collisions with neon ions

$$S_1 = \zeta_2 N_2/\tau_2 + \zeta_3 N_3/\tau_3 - k_{ct} N_1 N_3 ; \quad (7)$$

ζ_i being the sputtering coefficient of the ion i (ζ_2 includes copper atoms originating from recombined copper ions), and k_{ct} the charge transfer rate constant.

Copper ions are produced mainly by charge transfer collisions. There are no important losses except the diffusion to the walls

$$S_2 = k_{ct} N_1 N_3 . \quad (8)$$

Neon ions are produced by electron excitation, and they are annihilated by the charge transfer collisions

$$S_3 = R_{Ne} N_{Ne} - k_{ct} N_1 N_3 \quad (9)$$

where R_{Ne} is the ionization rate constant for neon, and $N_{Ne} = N_{Ne,0} - N_3$: the density of neon atoms ($N_{Ne,0}$ is proportional to the neon pressure).

From (4–9) we obtain

$$N_1'' + D_1' N_1'/D_1 - H A_1 N_1 + (H D_2 \zeta_2 N_2 + H D_3 \zeta_3 N_3 - k_{ct} N_1 N_3)/D_1 = 0 , \quad (10)$$

$$N_2'' + D_2' N_2'/D_2 - H N_2 + k_{ct} N_1 N_3/D_2 = 0 , \quad (11)$$

$$N_3'' + D_3' N_3'/D_3 - H N_3 + [R_{Ne}(N_{Ne,0} - N_3) - k_{ct} N_1 N_3]/D_3 = 0 . \quad (12)$$

This is a system of coupled nonlinear ordinary differential equations of second order, which has to be solved as a boundary problem. For that a numerical program based on the difference method [15] was used.

The following boundary conditions must be taken into account. No net particle flow in the axial direction can occur in the centre of the cathode ($x=0$) due to the symmetry. This results in $N_i'(0)=0$. Because, as in the experiment [5], the calculations are made for a single cathode (there are no neighbouring cathodes), the particle densities vanish at a certain distance x_m far enough from the cathode edge, i.e., $N_i(x_m)=0$. Because of the symmetry the calculation was made only for one half of the cathode starting from the centre ($x=0$) to the edge ($x=x_L=2$ cm) and up to $x=x_m$, which has been chosen as $x_m=3$ cm. One of the boundary conditions is outside the cathode requiring the knowledge of the particle densities outside the cathode, too. Thus one needs modified differential equations in this region:

The diffusion coefficients D_i are assumed to be constant ($D_i'=0$). Here the generation of copper atoms is not possible ($\zeta_i=0$), and the copper atoms are not reflected ($A_1=1$). However, neon atoms can be ionized, and charge transfer collisions can occur. The particle losses due to diffusion in radial directions are given approximately by the same terms as inside the cathode. Then the system of differential equations outside the cathode is

$$N_1'' - H N_1 - k_{ct} N_1 N_3/D_1 = 0 , \quad (13)$$

$$N_2'' - H N_2 + k_{ct} N_1 N_3/D_2 = 0 , \quad (14)$$

$$N_3'' - H N_3 + [R_{Ne}(N_{Ne,0} - N_3) - k_{ct} N_1 N_3]/D_3 = 0 . \quad (15)$$

After having calculated the particle densities by the solution of the system (10–15), the cathode erosion must be calculated. At first a particle flow density E_F from the cathode surface is introduced, which results from the difference between sputtered copper atoms and stuck copper atoms and copper ions

$$E_F = \zeta_2^* \Gamma_2 + \zeta_3 \Gamma_3 - A_1 \Gamma_1 - A_2 \Gamma_2 , \quad (16)$$

where Γ_i is the particle flow densities to the cathode surface, A_i the sticking coefficients, and ζ_2^* the sputtering coefficient excluding reflected copper atoms originating from recombined copper ions.

The particle flow densities striking the cathode surface result from the radial diffusion

$$\Gamma_i = V/A \cdot N_i/\tau_i = R/2 \cdot H D_i N_i , \quad (17)$$

where V is the volume of the cathode, and A the surface of the cathode.

As $\zeta_2^* - A_2 = \zeta_2 - 1$, we get from (16) and (17)

$$E_F = R/2 \cdot H[(\zeta_2 - 1) D_2 N_2 + \zeta_3 D_3 N_3 - A_1 D_1 N_1] . \quad (18)$$

From that the erosion rate E (decrease in the wall thickness per time) results as

$$E = E_F m_1/\varrho_1 , \quad (19)$$

where m_1 is the mass of one copper atom, and ϱ_1 the density of copper.

Parameters

The following parameters, for which values must be found depending on the experimental parameters, appear in (10–15, 18)

D_1, D_2, D_3,

A_1, ζ_2, ζ_3,

k_{ct}, R_{Ne}.

The charge transfer rate constant is according to [6 and 8] about $k_{ct} = 2 \cdot 10^{-9}$ cm^3/s, showing no dependence on the pressure or the current density.

The ionization rate constant for neon has been derived from the model of rate equations for mean particle densities. From (6) and (9) we obtain, neglecting the differential terms,

$$R_{Ne}=N_3(HD_3+k_{ct}N_1)/(N_{Ne,0}-N_3) \tag{20}$$

The numerical calculation of the rate equations (with (35) added for the current density j [A/cm^2] at the cathode surface) results in

$$R_{Ne}=280\,j\ [s^{-1}] \tag{21}$$

which is valid for $R=0.2$ cm and $p_{Ne}=8$ mbar.

Following the calculated values in [8], the sticking coefficient for copper atoms was used in the form of

$$A_1=0.05\,(1+10\,j)\,. \tag{22}$$

For the sputtering coefficient values are obtained from [9 and 11], assuming that the copper ions reach the cathode surface with the full energy of the cathode fall in contrast to the neon ions

$$\zeta_2=0.00603\cdot U-0.117\,, \tag{23}$$

with U being the discharge voltage [V] ($20\,V<U<350\,V$)

$$\zeta_3=1.2\cdot 10^{-5}E_3^2+1.4\cdot 10^{-3}E_3 \tag{24}$$

with E_3 being the energy of the neon ions striking the cathode wall [eV] ($E_3<200$ eV).

The following relations (25–28) are based on experimental data and theoretical considerations of other authors:

$$D_1=28.9/p_{Ne}\cdot T_{Gas}^{1/2}/(1+56/T_{Gas})\ [cm^2/s] \tag{25}$$

(p_{Ne}: neon pressure in mbar, T_{Gas}: gas temperature in K)

$$D_2=\mu_2(kT_{Gas}+E_e)/e\ [cm^2/s] \tag{26}$$

(e: elementary charge, k: Boltzmann's constant, E_e: mean thermal electron energy [J], $\mu_2=3.71\cdot 7/p_{Ne}\cdot T_{Gas}$: mobility of copper ions in neon [cm^2/(Vs)])

$$D_3=4/7\cdot D_2\,. \tag{27}$$

In (21–26) the terms j, T_{Gas}, E_e and E_3 appear, which must be expressed by experimental parameters, too. The energy of the neon ions at the cathode wall is

$$E_3=4.337\cdot 10^{17}\,m_3UT_{Gas}R^{-1/2}/k_h\ [eV] \tag{28}$$

(R: radius of the cathode [cm], m_3: mass of one neon ion [g], k_h: ratio between the thickness of the cathode layers in a hollow cathode discharge and in a normal glow discharge, $k_h=0.1$ is used).

The gas temperature and the electron energy are based on experiments in [8]. They can be expressed approximately as

$$T_{Gas}=700+1778\sqrt{j}+175\,j\ [K]\,, \tag{29}$$

$$E_e=1.602\cdot 10^{-19}\cdot(0.5+0.27\,p_{Ne})\sqrt{j}\ [J]\,. \tag{30}$$

The discharge voltage is $U=300$ V, if the experimental parameters are used as given in the introduction. For other values the voltage is approximated by means of experimental current-voltage characteristics given in [12 and 13]

$$U\approx\{184+200(R-0.1)+0.91\,p_{Ne} +[70+316\exp(-p_{Ne}/4)]j\}\cdot 1.38\,. \tag{31}$$

At first the current density at the cathode wall is assumed as a constant in the approximation procedure described below for the solution of the differential equations (Fig. 3)

$$j=I/A\,. \tag{32}$$

However, the current density depends on the x position, because it depends on the particle densities (which are functions of the x position) as follows. The flow density j/e of particles at the cathode surface is given by three different charged particle flow densities

$$\Gamma_e+\Gamma_2+\Gamma_3=j/e\,,$$
$$\Gamma_2 \text{ and } \Gamma_3 \text{ as in (17)}. \tag{33}$$

Γ_e is the electron flow density leaving the cathode surface. In the main it is caused by electron emission due to ion impact

$$\Gamma_e=\gamma_2\Gamma_2+\gamma_3\Gamma_3 \tag{34}$$

(γ_i: secondary electron emission coefficient).

From (17, 33 and, 34) follows

$$j=eR/2\cdot H[D_2(1+\gamma_2)N_2+D_3(1+\gamma_3)N_3]\,. \tag{35}$$

The electron emission coefficients were taken from [14]. No detail is given there for γ_2. Thus the values were obtained by interpolation from values of other particles

$$\gamma_2\approx 0.2+10^{-3}U\,, \tag{36}$$

$$\gamma_3=0.074+5.8\cdot 10^{-4}E_3\,. \tag{37}$$

Inserting the current density as given in (35–37) instead of (32), the system of differential equations (10–12) becomes still more nonlinear, because then the particle densities N_2 and N_3 are included in the parameters D_1, D_2, D_3, A_1, ζ_3, R_{Ne} and γ_3 in a multiple way.

Outside the cathode according to (13–15) only the parameters D_1, D_2, D_3, k_{ct} and R_{Ne} are required. For k_{ct}

the same constant value is used as inside the cathode. Also D_1, D_2, D_3 and R_{Ne} are assumed to be approximately constant outside the cathode having values, which result from the calculated values at the cathode edge.

Calculations

To solve the system of differential equations (10–15) using the difference method [15], the computer program needs the partial derivatives of all equations for each variable N_1, N_2, N_3 and for their derivatives N_1', N_2', N_3', N_1'', N_2'', N_3''. Further a 0^{th} approximation must be given for N_1, N_2, N_3, for example constant particle densities, which are calculated from the model of rate equations. At first it was tried to solve the system of differential equations in its more exact form, inserting the current density (35) which depends on x. This results in rather complicated terms for the partial derivatives mentioned above, and the equations could not be solved in spite of extensive variations of the parameters. Probably this is caused by the strong nonlinearities. Therefore some approximations had to be done.

In a first step only a weak dependence of the parameters on the position is assumed. That does mean the further use of x-dependent parameters in the differential equations, but calculating the partial derivatives of the equations the spatial dependence of the parameters was neglected. This approximation was not yet sufficient to get a solution.

Therefore, in a further approximation the parameters have been formulated inserting the constant current density (32). Thus solutions could be obtained for N_1, N_2 and N_3. Using these solutions $N_i(x)$ and the constant parameters, the resulting x-dependent current density $j(x)$ was calculated from (35) in the way shown in Fig. 3. Integrating over the cathode surface one obtains the total current I, which must be compared with the experimentally given value of I. If there are deviations, the calculation of N_1, N_2 and N_3 must be repeated using the constant current density multiplied by a correcting factor. In this way one obtains the first approximation of the cathode erosion rate $E(x)$ shown in Fig. 4a. In accordance with experiments, which always show a widening of cylindrical cathodes at the edges in the beginning, the computed erosion rate has the same behaviour.

Doing some more iteration steps, as shown in Fig. 3 (now starting with the first approximations of $j(x)$ and $N_i(x)$), the results for the erosion rate are not changed essentially. Therefore in the following the calculations are restricted to the first approximation.

The calculation, as described up to now, does not describe the formation of hollow spheres within the cylindrical cathode; a variation of the parameters only results in changes of the cathode erosion which do not match the experiments. On the other hand, it could not be expected, that the long time behaviour of the erosion can be described by a formalism, which is derived for the steady state in an undisturbed hollow cathode. To get further information, a disturbed case, as shown in Fig. 4a or Fig. 5a was taken as the starting position for the next step in the calculations.

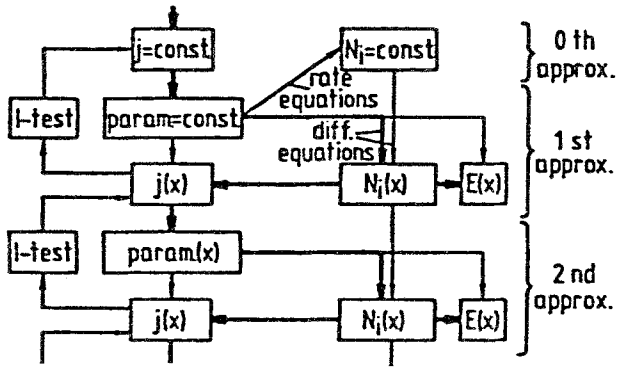

Fig. 3. Scheme of the iterative numerical solution of the system of differential equations (10–15)

After a certain period the conical widening of the bore in the edge region is connected with a change of the character of the discharge in this region: The hollow cathode effect decreases and tends to change into a normal glow discharge. A cone angle of about 6° is sufficient to disturb the hollow cathode effect. This view is supported by some experiments with short discharge tubes, whose active length (the total length of the cathodes) was just sufficient to obtain Cu*II* laser activity. After a weak conical widening of the bore at the cathode edges no lasing was possible. Obviously the active length with hollow cathode properties was shortened by the widening. Drilling a new hole made the cathode holes parallel again over their whole length, thus restoring laser activity.

Therefore in the calculation the change of the discharge is taken into account by deviding the cathode region from $x=0$ to $x=2$ cm into two parts, the inner one with the hollow cathode effect as before up to $x=1.65$ cm and the outer one with a disturbed hollow cathode discharge. This region is characterized by a thicker cathode fall ($k_h \approx 1$ in (28)) and by a smaller ionization rate of neon. In comparison with the hollow cathode discharge, R_{Ne} has been decreased by a factor of $0.5-0.1$ in the calculation. The radius R of the cathode has been left constant in the calculation, because little deviations from parallelism should not have a remarkable effect on the radial diffusion modes. In principle, the calculations result in a cathode erosion rate as shown in Fig. 4b. In this case the ionization constant R_{Ne} was decreased only by a factor

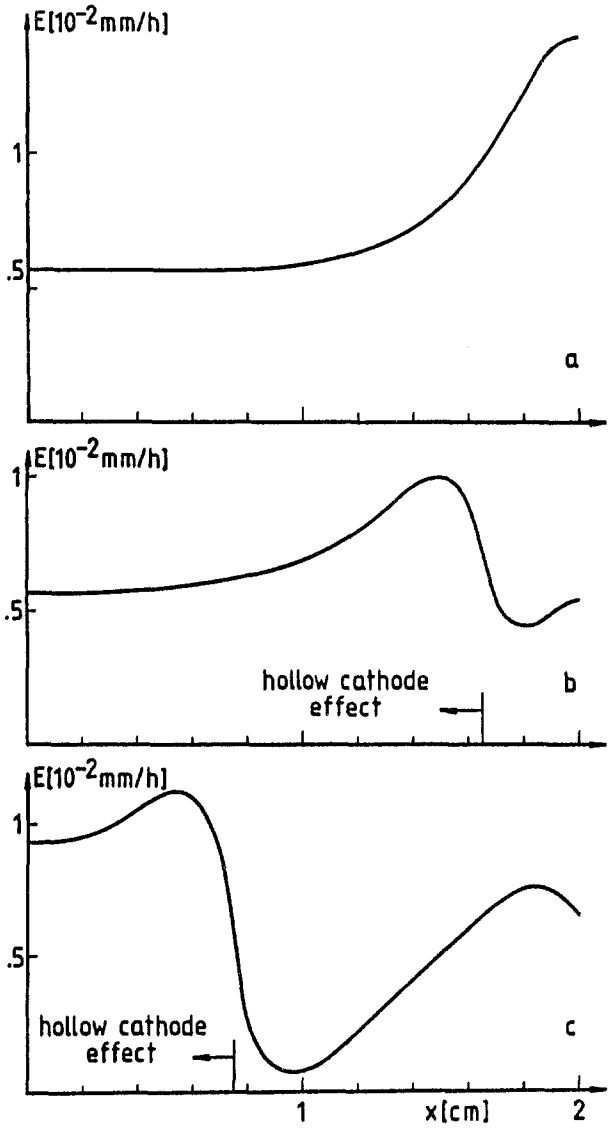

Fig. 4a–c. Erosion rate of a cylindrical hollow cathode in dependence on the axial direction. The calculation has been made for a cathode diameter of $2R=0.4$ cm, a neon pressure of $p_{Ne}=8$ mbar, a discharge current of $I=0.3$ A and a discharge voltage of $U=300$ V. (a) Hollow cathode effect all over the cathode (up to $x=2$ cm); (b) Hollow cathode effect up to $x=1.65$ cm; (c) Hollow cathode effect up to $x=0.75$ cm

of 0.5. At the assumed boundary – which in reality is a transition zone – the erosion rate has a point of inflection. In the adjacent hollow cathode region the erosion rate E has a maximum, and in the adjacent disturbed hollow cathode discharge it has a minimum showing either a small erosion rate or a deposition of material (after some iteration steps or with somewhat different parameters). An erosion rate, as shown in Fig. 4b, can lead to the development of a bulge, situated at the erosion rate maximum next to the broadened edge region of the cylindrical cathode.

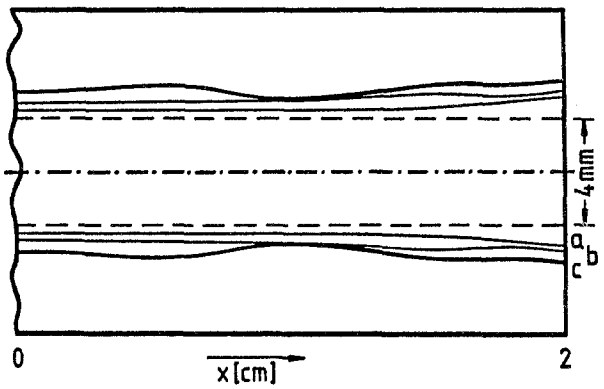

Fig. 5a–c. Calculated longitudinal section of the cathode shown in Fig. 1. (a) After 50 h erosion according to Fig. 4a; (b) After additional 50 h erosion according to Fig. 4b; (c) After additional 50 h erosion according to Fig. 4c

The position of the boundary was chosen somewhat arbitrary, to deliver an erosion curve corresponding to experimental observation in one step. In reality the boundary or transition zone will shift continuously from the edge in the negative x direction, in the course of which the erosion rate curve in Fig. 4a develops into a shape of the type in Fig. 4b. But this shift slows down, when a conical region open to the center emerges and subsequently the bulge is growing. At the same time on the other side of the bulge a conical region open to the edge develops with the consequence, that a new region with a changed character of the discharge develops. In the center of the bulge the hollow cathode effect is stable.

In a further calculation the corresponding new boundary of the region with the hollow cathode effect was set at $x=0.75$ cm. Its continuous shift phase was omitted again. The hollow cathode effect inside the centre of the first bulge has been neglected in this calculation. It gives an erosion rate curve, as shown in Fig. 4c, which leads to the development of the next bulge further inwards.

Figure 5 shows the calculated change in the longitudinal section of the cathode corresponding to that in Fig. 1. In a rough approximation it is assumed, that the cathode has been eroded each time for 50 h according to Figs. 4a–c. Considering the variation in the experimental results (Fig. 1) and considering the lot of approximations made in the calculation, the comparison of curve c in Fig. 5 with the experiment (Fig. 1) shows a satisfactory correspondence.

In this way one can derive a structure in long cylindrical hollow cathodes, which is the starting point for the further distortion of the small bulges into hollow spheres. Different mechanisms can influence this further distortion. It could be favoured by the described formation of an erosion maximum and an

erosion minimum next to the boundary between a hollow cathode discharge and a disturbed hollow-cathode discharge. But moreover the effect of the changing geometry on the diffusion becomes important. In addition, a different microstructure of the cathode surface develops in regions with strong erosion and in regions with weak erosion or deposition of material. A strong erosion results in a rougher surface [5], which leads to a greater sputtering coefficient than in a deposition area [11]. This favours the formation of hollow spheres, too.

Finally the experimental parameters were varied in the calculation to a little extent. Decreasing the length of the cathode from $L=4$ cm to $L=1.6$ cm, which is done with a constant current density (i.e., $I=0.12$ A), an erosion rate maximum is obtained in the centre of the cathode, which is the experimental result in [5], too. Increasing the current from 0.3 to 1.5 A for $L=4$ cm again, this results in nearly the same shape of the erosion rate curves, as shown in Fig. 4, but the erosion is about 5 times faster. A change of the neon pressure from 8 to 12 mbar has no effect.

Conclusions

The presented calculations indicate, that the structuring of cylindrical hollow cathodes (Fig. 1), which leads to the formation of hollow spheres, is caused by the development of conical regions with a disturbed hollow cathode discharge. At first such conical regions arise from the edges of the hollow cathode, due to the different drop of the different particle types from the centre of the cathode to the outside. Then inside the cathode further conical regions can develop. This is caused by the formation of erosion maxima and minima next to the boundary of the outer conical regions. Therefore, one must conclude that the geometry of hollow cathodes is always changed, as long as losses of particles are possible. Only in a closed or nearly closed system, like in a hollow sphere with a small aperture [3, 5], perhaps a stable geometry is possible, showing no or only a scaled change in the cathode geometry.

References

1. G. Knerr, J. Maierhofer, A. Reis: Z. Anal. Chem. **229**, 241 (1967)
2. H.J. Eichler, H. Koch, J. Salk, Ch. Skrobol: Opt. Commun. **34**, 228 (1980)
3. A.D. White: J. Appl. Phys. **30**, 711 (1959)
4. E.H. Daughtrey, D.L. Donohue, P.J. Slevin, W.W. Harrison: Anal. Chem. **47**, 683 (1975)
5. H.J. Eichler, H. Koch, R. Tornow: Proc. 6th Int. Congr. Laser **83**, 14 (1984)
6. B.E. Warner, K.B. Persson, G.J. Collins: J. Appl. Phys. **50**, 5694 (1979)
7. H. Koch, H.J. Eichler: J. Appl. Phys. **54**, 4939 (1983)
8. E.M. van Veldhuizen: Dissertation, Technische Hogeschool Eindhoven (1983)
9. H. Koch: Dissertation, Technische Universität Berlin (1982)
10. B.E. Cherrington: *Gaseous Electronics and Gas Lasers* (Pergamon, Oxford 1979)
11. R. Behrisch (ed): *Sputtering by Particle Bombardement I*, Topics Appl. Phys. **47** (Springer, Berlin, Heidelberg 1981)
12. H.J. Eichler, H. Koch, J. Salk, G. Schäfer: IEEE. J. QE-**15**, 908 (1979)
13. H. Koch: Diplomarbeit, Technische Universität Berlin (1978)
14. M. von Ardenne: *Tabellen zur angewandten Physik I* (VEB Deutscher Verlag der Wissenschaften, Berlin 1962) p. 110
15. G. Glotz, W. Schoenauer, K. Raith: *SLGR — Ein Programmpaket zur selbstadaptiven Berechnung von Randwertproblemen bei gewöhnlichen Differentialgleichungen 2. Ordnung*, Rechenzentrum Universität Karlsruhe, interner Bericht 20/81